International Journal of Mechanical, Industrial and Aerospace Sciences
ISSN: 2517-9950
Vol:3, No:3, 2009

Bond Graph Modeling of Mechanical Dynamics of an Excavator for Hydraulic System Analysis and Design

Mutuku Muvengei and John Kihiu,

Abstract—This paper focuses on the development of bond graph dynamic model of the mechanical dynamics of an excavating mechanism previously designed to be used with small tractors, which are fabricated in the Engineering Workshops of Jomo Kenyatta University of Agriculture and Technology. To develop a mechanical dynamics model of the manipulator, forward recursive equations similar to those applied in iterative Newton-Euler method were used to obtain kinematic relationships between the time rates of joint variables and the generalized cartesian velocities for the centroids of the links. Representing the obtained kinematic relationships in bond-graphic form, while considering the link weights and momenta as the elements led to a detailed bond graph model of the manipulator. The bond graph method was found to reduce significantly the number of recursive computations performed on a 3 DOF manipulator for a mechanical dynamic model to result, hence indicating that bond graph method is more computationally efficient than the Newton-Euler method in developing dynamic models of 3 DOF planar manipulators. The model was verified by comparing the joint torque expressions of a two link planar manipulator to those obtained using Newton-Euler and Lagrangian methods as analyzed in robotic textbooks. The expressions were found to agree indicating that the model captures the aspects of rigid body dynamics of the manipulator. Based on the model developed, actuator sizing and valve sizing methodologies were developed and used to obtain the optimal sizes of the pistons and spool valve ports respectively. It was found that using the pump with the sized flow rate capacity, the engine of the tractor is able to power the excavating mechanism in digging a sandy-loom soil.

Keywords—Actuators, bond graphs, inverse dynamics, recursive equations, quintic polynomial trajectory.

I. Introduction

IN order to design, improve performance, simulate the behavior and finally control a system or plant, it is necessary to obtain it's dynamics. To develop the dynamics of a manipulator, a kinematic model of the manipulator is required first. The kinematic modeling is done first by attaching coordinate frames to every link. The usual convention applied to attach frames in the links of a manipulator is the Denavit-Hartenberg procedure [1]. The dynamics of a manipulator can be modeled using various methods namely; Newton-Euler formulation, Lagrangian formulation, Kane's method, and others [2], [3].

The three methods; Newton-Euler, Lagrangian and Kane's methods tend to hide the physical interactions between the elements involved [4]. The relatively new bond graph modeling technique, has been proposed to successfully model the dynamics of manipulators and mechanisms. Since bond graph method is based on the interaction of power between elements, it can be used to model multi-energy domains also, for example the actuator system of the manipulator which may be electrical, pneumatic, hydraulic or mechanical. Once the bond graph model is ready, the system equations can be derived from it algorithmically in a systematic manner. This process is usually automated using appropriate softwares such as ENPORT, CAMP-G, TUTSIM 20-SIM, SYMBOLS 2000, etc which support bond graphs. For mechanical manipulators and mechanisms, the bond graph model can be developed based on kinematic relationships between the time rates of joint variables and the generalized cartesian velocities (translational and angular velocities). It is not necessary to have higher order time rates of variables involved, that is translational and angular accelerations.

The concept of bond graphs was originated by Paynter [5]. The idea was further developed by Karnopp and Rosenberg in their textbooks [6]–[8], such that it could be used in practice. By means of the formulation by Breedveld [9] of a framework based on thermodynamics, bond graph model description evolved to a systems theory. More information about bond graphs can be found in [6]–[12].

The Bond graph method can be used to obtain more intricate information such as the power required to drive each joint actuator, or the power interaction at the interface with the environment. Such information can also be used to study the stability of the manipulator system during contact interaction with the environment. Modifications and additions to the system can be easily incorporated by connecting suitable bond-graphic sub-systems to its existing bond graph.

In this paper, the mechanical dynamics of the excavating manipulator designed in [13] to be used with the small tractors (fabricated in the Engineering Workshops of Jomo Kenyatta University of Agriculture and Technology) in digging medium-height trenches for small scale farmers, is modeled using the bond graph method. The excavating manipulator is shown in Fig. 1. Inverse dynamics is performed on the developed dynamic model for purposes of analyzing the hydraulic system design.

In this work, forward recursive equations for motion of manipulators similar to those used in Newton-Euler method are used to derive the kinematic relationships between the time rates of joint variables, and the generalized cartesian velocities

M. Muvengei is with the Department of Mechanical Engineering, Jomo Kenyatta University of Agriculture and Technology, P.O BOX 62000-00200 Kenya (Tel: +254720642441, e-mail: mmuvengei@eng.jkuat.ac.ke.)

J. Kihiu is with the Department of Mechanical Engineering, Jomo Kenyatta University of Agriculture and Technology, P.O BOX 62000-00200 Kenya (email: kihiusan@yahoo.com)

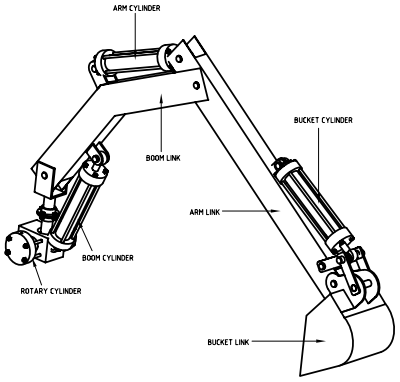

Fig. 1. Schematic drawing of a part of assembled excavator

(translational and angular velocities) of mass centers of the links. These kinematic relations are further used for graphical representation of the system dynamics using Bond graphs.

II. Modeling the Manipulator Dynamics

Assuming that; the inertial effects of cylinders and their pistons are negligibly small compared to those of manipulator links, the hydraulic cylinders transmit axial forces only, the revolute joints have no friction, and all the links and supports are rigid, a bond graph model representing the mechanical dynamics of the excavating manipulator was developed.

A. Kinematic Analysis and Forward Recursion

Kinematic analysis was performed on the excavating manipulator to relate the translational velocities of the center of masses of the links (v_{Gi}) to the time rates of the joint variables $(\dot{\theta}_i)$, for $i = 2, 3, 4$. The choice of center of mass velocities for rigid bodies leads to a highly systematic approach for constructing bond graphs and is recommended [7].

The homogeneous transformation matrices (1) to (4) were obtained by first attaching world coordinate frames to the three links as shown Fig. 2 by using Denavit-Hartenberg procedure as described in [14].

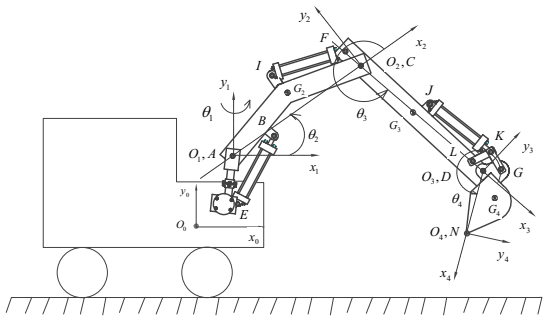

Fig. 2. Coordinate System assignment for excavator.

$$A_0^{(1)} = \begin{pmatrix} \cos\theta_1 & -\sin\theta_1 & 0 & a_1\cos\theta_1 \\ \sin\theta_1 & \cos\theta_1 & 0 & a_1\sin\theta_1 \\ 0 & 0 & 1 & 0 \\ 0 & 0 & 0 & 1 \end{pmatrix} \quad (1)$$

$$A_1^{(2)} = \begin{pmatrix} \cos\theta_2 & -\sin\theta_2 & 0 & a_2\cos\theta_2 \\ \sin\theta_2 & \cos\theta_2 & 0 & a_2\sin\theta_2 \\ 0 & 0 & 1 & 0 \\ 0 & 0 & 0 & 1 \end{pmatrix} \quad (2)$$

$$A_2^{(3)} = \begin{pmatrix} \cos\theta_3 & -\sin\theta_3 & 0 & a_3\cos\theta_3 \\ \sin\theta_3 & \cos\theta_3 & 0 & a_3\sin\theta_3 \\ 0 & 0 & 1 & 0 \\ 0 & 0 & 0 & 1 \end{pmatrix} \quad (3)$$

$$A_3^{(4)} = \begin{pmatrix} \cos\theta_4 & -\sin\theta_4 & 0 & a_4\cos\theta_4 \\ \sin\theta_4 & \cos\theta_4 & 0 & a_4\sin\theta_4 \\ 0 & 0 & 1 & 0 \\ 0 & 0 & 0 & 1 \end{pmatrix} \quad (4)$$

Kinematic relationships between the translational velocities of the center of masses of the links (v_{Gi}) to the time rates of the joint variables $(\dot{\theta}_i)$ (where $i = 2, 3, 4$) can be obtained by using forward recursive equations which were proposed by Luh et al. [15]. The translational velocity v_{Gi}^i of the center of mass of the i^{th} link as specified in the i^{th} coordinate frame is given recursively by;

$$v_{Gi}^{(i)} = v_{0i}^{(i)} + \omega_i^{(i)} \times (P_{Gi}^{(i)} - P_{0i}^{(i)}) \quad (5)$$

Where

- $P_{Gi}^{(i)}$ is the vector from the origin of the base coordinate system to the center of mass of the i^{th} frame as expressed in the i^{th} coordinate system.
- $P_{0i}^{(i)}$ is the vector from the origin of the base coordinate system to the origin of the i^{th} coordinate system as expressed in the i^{th} coordinate system.
- $\omega_i^{(i)}$ is the rotational velocity of link i as specified in the i^{th} coordinate frame, and is given recursively as;

$$\omega_i^{(i)} = R_i^{(i-1)}\omega_{i-1}^{(i-1)} + \dot{Z}_0\dot{q}_i \quad (6)$$

  where
  - $R_i^{(i-1)}$ is the rotational matrix relating two adjacent frames and is obtained from the respective homogeneous transformation matrix.
  - $\dot{Z}_0 = \begin{pmatrix} 0 \\ 0 \\ 1 \end{pmatrix}$
  - $\dot{q}_i = \dot{\theta}_i$ for revolute joints.
- $v_{0i}^{(i)}$ is the translational velocity of the origin of the i^{th} link coordinate frame as expressed in the i^{th} coordinate frame and is given recursively as,

$$v_{0i}^{(i)} = R_i^{(i-1)}v_{0i-1}^{(i-1)} + \omega_i^{(i)} \times (P_{0i}^{(i)} - P_{0i-1}^{(i)}) \quad (7)$$

  where
  - $P_{0i-1}^{(i)}$ is the vector from the origin of the base coordinate system to the origin of the $(i-1)^{th}$ coordinate system as expressed in the i^{th} coordinate system.
  - $P_{0i}^{(i)}$ is the vector from the origin of the base coordinate system to the origin of the i^{th} coordinate system as expressed in the i^{th} coordinate system.

B. Modeling the Bucket Digging Force

A model that accounts for the material being retained in the bucket, which was developed by Cannon [16] using force equilibrium and fundamental earthmoving equation in soil mechanics was applied in this study to determine the force F exerted by the excavator bucket to the soil. From Fig. 3, the force F is given in (8).

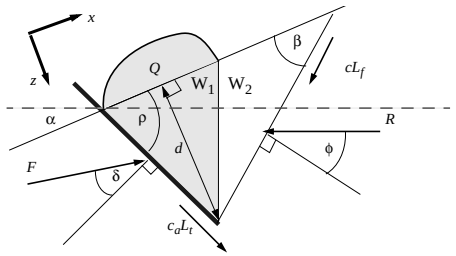

Fig. 3. Wedge model that accounts for the material being retained in the bucket.

$$F = d^2 w\gamma g N_w + cwdN_c + V_s\gamma g N_q \tag{8}$$

V_s is the swept volume, Q is the surcharge, W_1 is the weight of the material above the bucket, W_2 is the weight of the rest of material in the wedge, L_t is the length of the tool, L_f is the length of the failure surface, R is the force of the soil resisting the moving of the wedge, F is the force exerted by the tool on the wedge, c_a is the adhesion between the soil and the blade, c is the cohesiveness of the soil media, β is the failure surface angle (slip angle), α is the surface terrain slope (cutting angle), ϕ is the soil-soil friction angle, ρ is the rake angle of the tool relative to the soil surface, σ is the soil-tool friction angle, d is the depth of the bucket tool perpendicular to the soil surface, w is the width of the bucket, γ is the bulk density of the soil media and g is the gravitational acceleration.

N_w, N_c N_q are N-factors which depend on: the soil's frictional strength, the bucket tool geometry and soil-to-tool strength properties, and are given by the following equations.

$$N_w = \frac{\Big(\cot\beta - \tan\alpha\Big)\Big(\cos\alpha + \sin\alpha\cot(\beta+\phi)\Big)}{2\Big(\cos(\rho+\sigma) + \sin(\rho+\sigma)\cot(\beta+\phi)\Big)} \tag{9}$$

$$N_c = \frac{1 + \cot\beta\cot(\beta+\phi)}{\cos(\rho+\sigma) + \sin(\rho+\sigma)\cot(\beta+\phi)} \tag{10}$$

$$N_q = \frac{\cos\alpha + \sin\alpha\cot(\beta+\phi)}{\cos(\rho+\sigma) + \sin(\rho+\sigma)\cot(\beta+\phi)} \tag{11}$$

Equations (8) to (11) show that the magnitude of the digging force depends on many factors such as the cutting angle, specific resistance to cutting, volume of the bucket, amount of the the material ripped into the bucket and the volume of the material surcharged. These factors are always varying during the bucket digging operation and indicate complicated interactions of the bucket and the soil, hence making modeling of the bucket digging force throughout the digging process a complex and bulk process.

In this study, a simplified model is presented by considering the situation of critical force, and then assuming the force to remain constant throughout the digging process. The critical value of the cutting angle is given by [17],

$$\alpha_c = \frac{1}{2}\Big(\pi - \sigma - \sin^{-1}(\sin\sigma\sin\rho)\Big) \tag{12}$$

The soil-tool force F is assumed to be applied at the cutting edge of the bucket. From the Newton's third law of motion, the soil applies an opposite and equal reaction force at the bucket, which can be resolved to a normal and tangential force components as shown in Fig. 4

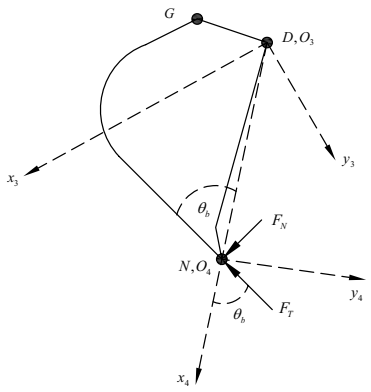

Fig. 4. Bucket digging force at the tip.

The horizontal and vertical components of the bucket reaction force are given as;

$$\begin{aligned} F_x = &-(F_T\cos\theta_b - F_N\sin\theta_b)\cos(\theta_2+\theta_3+\theta_4) \\ &+(F_T\sin\theta_b + F_N\cos\theta_b)\sin(\theta_2+\theta_3+\theta_4) \end{aligned} \tag{13}$$

$$\begin{aligned} F_y = &-(F_T\cos\theta_b - F_N\sin\theta_b)\sin(\theta_2+\theta_3+\theta_4) \\ &-(F_T\sin\theta_b + F_N\cos\theta_b)\cos(\theta_2+\theta_3+\theta_4) \end{aligned} \tag{14}$$

These forces are included at the translational velocity of the origin of the 4^{th} link coordinate frame but referenced to the base coordinate frame.

C. Overall Bond Graph Model of the Manipulator

The kinematic relationship obtained from (5) for each link was represented in bond-graphic form while considering the weights and momenta of the links as the bond graph elements. All the bond graph sub-models were then assembled to an overall non causal bond graph of the manipulator as shown in Fig. 5.

Where

- $r_1 = L_{G_2O_2}\sin(\theta_2 - \sigma_1) - L_{O_1O_2}\sin\theta_2$
- $r_2 = -L_{G_2O_2}\cos(\theta_2 - \sigma_1) + L_{O_1O_2}\cos\theta_2$
- $r_3 = -L_{O_1O_2}\sin\theta_2 + L_{G_3O_3}\sin(\theta_2+\theta_3-\sigma_2) - L_{O_2O_3}\sin(\theta_2+\theta_3)$
- $r_4 = -L_{G_3O_3}\sin(\theta_2+\theta_3-\sigma_2) + L_{O_2O_3}\sin(\theta_2+\theta_3)$
- $r_5 = L_{O_1O_2}\cos\theta_2 - L_{G_3O_3}\cos(\theta_2+\theta_3-\sigma_2) + L_{O_2O_3}\cos(\theta_2+\theta_3)$
- $r_6 = -L_{G_3O_3}\cos(\theta_2+\theta_3-\sigma_2) + L_{O_2O_3}\cos(\theta_2+\theta_3)$
- $r_7 = -L_{O_1O_2}\sin\theta_2 - L_{O_2O_3}\sin(\theta_2+\theta_3) - L_{O_3O_4}\sin(\theta_2+\theta_3+\theta_4) + L_{G_4O_4}\sin(\theta_2+\theta_3+\theta_4-\sigma_3)$

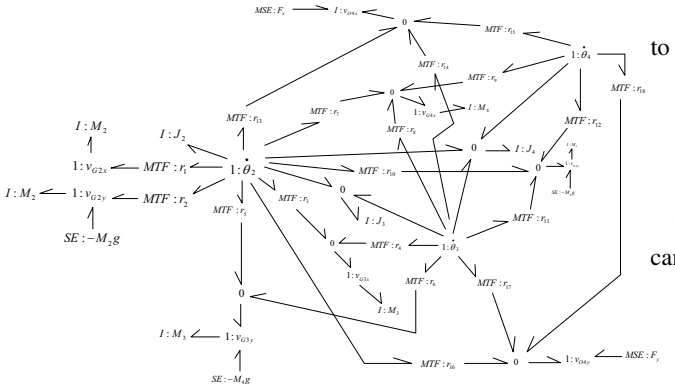

Fig. 5. A non causal bond graph model representing the mechanical dynamics of the manipulator.

- $r_8 = -L_{O_2O_3}\sin(\theta_2+\theta_3) - L_{O_3O_4}\sin(\theta_2+\theta_3+\theta_4) + L_{G_4O_4}\sin(\theta_2+\theta_3+\theta_4-\sigma_3)$
- $r_9 = -L_{O_3O_4}\sin(\theta_2+\theta_3+\theta_4) + L_{G_4O_4}\sin(\theta_2+\theta_3+\theta_4-\sigma_3)$
- $r_{10} = L_{O_1O_2}\cos\theta_2 + L_{O_2O_3}\cos(\theta_2+\theta_3) + L_{O_3O_4}\cos(\theta_2+\theta_3+\theta_4) - L_{G_4O_4}\cos(\theta_2+\theta_3+\theta_4-\sigma_3)$
- $r_{11} = L_{O_2O_3}\cos(\theta_2+\theta_3) + L_{O_3O_4}\cos(\theta_2+\theta_3+\theta_4) - L_{G_4O_4}\cos(\theta_2+\theta_3+\theta_4-\sigma_3)$
- $r_{12} = L_{O_3O_4}\cos(\theta_2+\theta_3+\theta_4) - L_{G_4O_4}\cos(\theta_2+\theta_3+\theta_4-\sigma_3)$
- $r_{13} = -L_{O_1O_2}\sin\theta_2 - L_{O_2O_3}\sin(\theta_2+\theta_3) - L_{O_3O_4}\sin(\theta_2+\theta_3+\theta_4)$
- $r_{14} = -L_{O_2O_3}\sin(\theta_2+\theta_3) - L_{O_3O_4}\sin(\theta_2+\theta_3+\theta_4)$
- $r_{15} = -L_{O_3O_4}\sin(\theta_2+\theta_3+\theta_4)$
- $r_{16} = L_{O_1O_2}\cos\theta_2 + L_{O_2O_3}\cos(\theta_2+\theta_3) + L_{O_3O_4}\cos(\theta_2+\theta_3+\theta_4)$
- $r_{17} = L_{O_2O_3}\cos(\theta_2+\theta_3) + L_{O_3O_4}\cos(\theta_2+\theta_3+\theta_4)$
- $r_{18} = L_{O_3O_4}\cos(\theta_2+\theta_3+\theta_4)$

D. Checking the Model

One way to check the bond graph model developed in Fig. 5 is to compare results with those available in the literature. A two link manipulator shown in Fig. 6, moving in a free space, and whose links are uniform and of equal lengths was considered. Such a problem is studied using Newton-Euler, Lagrangian, and d'Alembert's methods in the standard robotic textbooks [2], [3].

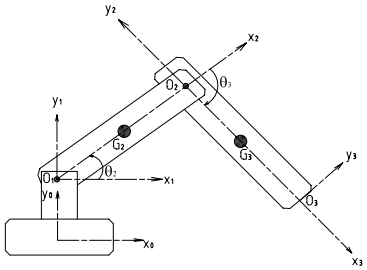

Fig. 6. A two link planar manipulator.

All the rotation axes at the joints are along the z-axis normal to the paper surface. Let;

$$\begin{aligned} L_{O_1O_2} &= L_{O_2O_3} = l \\ L_{G_2O_2} &= L_{G_3O_3} = \frac{l}{2} \\ \sigma_1 &= \sigma_2 = 0 \end{aligned}$$

The bond graph model of the two link planar manipulator can be represented as shown in Fig. 7;

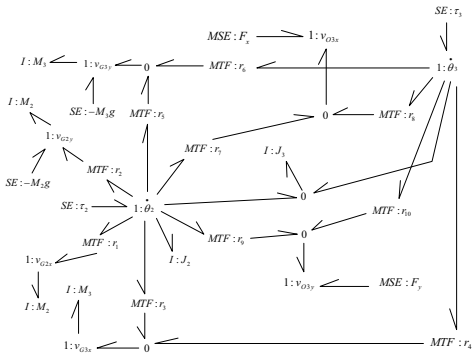

Fig. 7. A non causal bond graph model representing the mechanical dynamics of a 2-link manipulator.

Where,

- $r_1 = -\frac{l}{2}\sin\theta_2$
- $r_2 = \frac{l}{2}\cos\theta_2$
- $r_3 = -l\sin\theta_2 - \frac{l}{2}\sin(\theta_2+\theta_3)$
- $r_4 = -\frac{l}{2}\sin(\theta_2+\theta_3)$
- $r_5 = l\cos\theta_2 + \frac{l}{2}\cos(\theta_2+\theta_3)$
- $r_6 = \frac{l}{2}\cos(\theta_2+\theta_3)$
- $r_7 = -l\sin\theta_2 - l\sin(\theta_2+\theta_3)$
- $r_8 = -l\sin(\theta_2+\theta_3)$
- $r_9 = l\cos\theta_2 + l\cos(\theta_2+\theta_3)$
- $r_{10} = l\cos(\theta_2+\theta_3)$

The joint torques applied to each of the joint by the respective actuator can be obtained systematically from the bond graph using the constitutive relations, and noting that $F_x = F_y = 0$ since the manipulator is moving in free space. The external torque applied to move link 3 can be obtained from the bond graph as;

$$\begin{aligned} \tau_3 &= \frac{1}{3}m_3l^2\ddot{\theta}_2 + \frac{1}{3}m_3l^2\ddot{\theta}_3 + \frac{1}{2}m_3l^2\ddot{\theta}_2\cos\theta_3 + \frac{1}{2}m_3l^2\dot{\theta}_2^2 \\ &\quad \sin\theta_3 + \frac{1}{2}m_3gl\cos(\theta_2+\theta_3) \end{aligned} \tag{15}$$

The external torque applied to move link 2 can be obtained from the bond graph as;

$$\begin{aligned} \tau_2 = &\frac{1}{3}m_2l^2\ddot{\theta}_2 + \frac{4}{3}m_3l^2\ddot{\theta}_2 + \frac{1}{3}m_3l^2\ddot{\theta}_3 + m_3l^2\ddot{\theta}_2\cos\theta_3 \\ &+\frac{1}{2}m_3l^2\ddot{\theta}_3\cos\theta_3 - m_3l^2\dot{\theta}_2\dot{\theta}_3\sin\theta_3 - \frac{1}{2}m_3l^2\dot{\theta}_2^2\sin\theta_3 \\ &+\frac{1}{2}m_2gl\cos\theta_2 + m_3gl\cos\theta_2 + \frac{1}{2}m_3g\cos(\theta_2+\theta_3) \end{aligned} \tag{16}$$

The equations of external torque given in (15) and (16) correspond to those obtained using Newton-Euler and Lagrangian

methods for the same planar manipulator, as illustrated in [2], [3]. This indicates that, the model developed captures the essential aspects of rigid body dynamics of the manipulator.

III. Hydraulic System Analysis and Design Using Inverse Dynamics

In inverse dynamics, the generalized joint torques are computed given the desired joint trajectories. The joint trajectories are obtained through the trajectory planning schemes which generally interpolate or approximate the desired manipulator path by a class of polynomial functions and generates a sequence of time-based set-points for the manipulator from the initial position and orientation to its destination [2].

Quintic trajectory is used to size the spool valves and the pistons of the hydraulic cylinders, and also to check the total power required when the bucket of the manipulator is digging a sandy-loom soil. As described in [16], all the cylinders will be considered to be extending simultaneously during the digging operation.

Model parameters are needed to run simulations. Parameters like lengths, masses and angles were found from design drawings and trigonometric calculations. But parameters like the location of a center of mass, link moments of inertia, products of inertia of a link could not be estimated from blueprints. Auto CAD with Advanced Modeling Extension Package was used to estimate the mass properties of all the links and the locations of center of masses.

A. Trajectory Planning

In a typical trajectory, all joints move simultaneously. For the typical trajectory selected here, the boom, arm, and bucket links move from their minimum to maximum positions and all joints start and finish moving at the same time, although different time limits can be programmed.

Three common trajectories namely, trapezoidal trajectory, cubic polynomial trajectory, and quintic polynomial trajectory have been previously applied in trajectory planning for hydraulic manipulators. Sarkar [18] used the three trajectories to size the valves and power requirement for an articulated forestry machine. Among the three methods, the quintic polynomial trajectory has advantage in that;

- the velocity trajectory is smooth unlike in trapezoidal trajectory whose velocity profile has discontinuities where the link motion starts to settle at a constant velocity, and where the link starts to decelerate.
- the acceleration profile has values equal to zero at starting and finishing times of the trajectory, unlike in the other trajectories where the acceleration values at the start and final times have non zero values.

Therefore the trajectory to be adopted in this work is the quintic polynomial trajectory which is given by;

$$x(t) = a_0 + a_1 t + a_2 t^2 + a_3 t^3 + a_4 t^4 + a_5 t^5 \qquad (17)$$

The desired boundary conditions are; $x_{t=0} = x_{min}$, $x_{t=t_f} = x_{max}$, $\dot{x}_{t=0} = 0$, $\dot{x}_{t=t_f} = 0$, $\ddot{x}_{t=0} = 0$ and $\ddot{x}_{t=t_f} = 0$. By taking the first and second derivatives of (17) and satisfying these boundary conditions, the coefficients of the polynomial can be obtained and substituted in the polynomial equation (17) to get the required displacement, velocity and acceleration trajectories as;

$$x(t)=x_{min} + \frac{10(x_{max} - x_{min})}{t_f^3} t^3 + \frac{15(x_{min} - x_{max})}{t_f^4} t^4 + \frac{6(x_{max} - x_{min})}{t_f^5} t^5 \qquad (18)$$

$$\dot{x}(t)=\frac{30(x_{max} - x_{min})}{t_f^3} t^2 + \frac{60(x_{min} - x_{max})}{t_f^4} t^3 + \frac{30(x_{max} - x_{min})}{t_f^5} t^4 \qquad (19)$$

$$\ddot{x}(t)=\frac{60(x_{max} - x_{min})}{t_f^3} t + \frac{180(x_{min} - x_{max})}{t_f^4} t^2 + \frac{120(x_{max} - x_{min})}{t_f^5} t^3 \qquad (20)$$

B. Simulink Model for the Inverse Dynamics of the 3 dof System

In Fig. 8, the complete Simulink model of the inverse dynamics of 3dof excavating manipulator is shown. This model is the test-bed for all inverse dynamics simulations done on the system. The whole system is run in the same time frame, and as a result the outputs must match the generated trajectories.

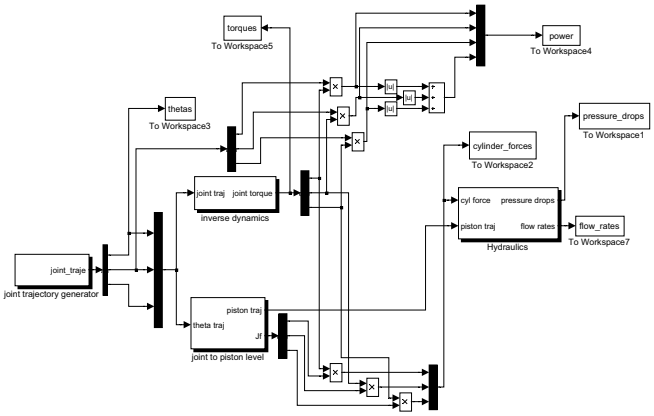

Fig. 8. The overall Simulink block for the inverse dynamics

The *joint trajectory generator block* produces the desired boom, arm and bucket quintic polynomial trajectories, that is, the angular displacements, angular velocities and angular accelerations of the links according to (18)-(20). The three signals from the *joint trajectory generator block* each containing the corresponding signals for the boom, arm and bucket link are fed into the *inverse dynamics block* to compute the joint torques for the bucket, arm and boom links respectively. The joint torque profiles when the bucket is digging a sandy-loom soil is shown in Fig. 9.

C. Power Profiles

The dynamic model obtained also permits either sizing of the system power supply or checking whether the desired

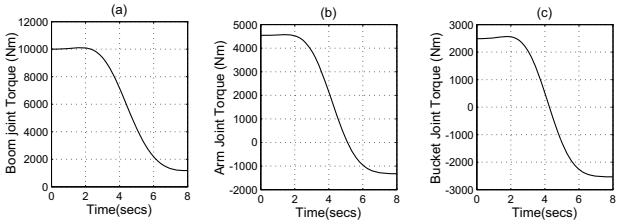

Fig. 9. The torque profiles at manipulator joints, when the bucket is digging a sandy-loom soil; **(a)** Boom joint torque **(b)** Arm joint torque **(c)** Bucket joint torque

manipulator trajectory can be followed without exceeding the power capacity of the supply. The power required for the boom, arm and bucket motion is respectively given as;

$$P_{bo} = \tau_{bo}\dot{\theta}_2 \quad (21)$$

$$P_a = \tau_a\dot{\theta}_3 \quad (22)$$

$$P_{bu} = \tau_{bu}\dot{\theta}_4 \quad (23)$$

Where τ is the torque required to move a link at an angular velocity of $\dot{\theta}$. The total power required for a given trajectory can be obtained by;

$$P_{total} = |P_{bo}| + |P_a| + |P_{bu}| \quad (24)$$

assuming there are no power losses. The power requirement profiles for the manipulator are given in Fig. 10 when the bucket is digging a sandy-loom soil.

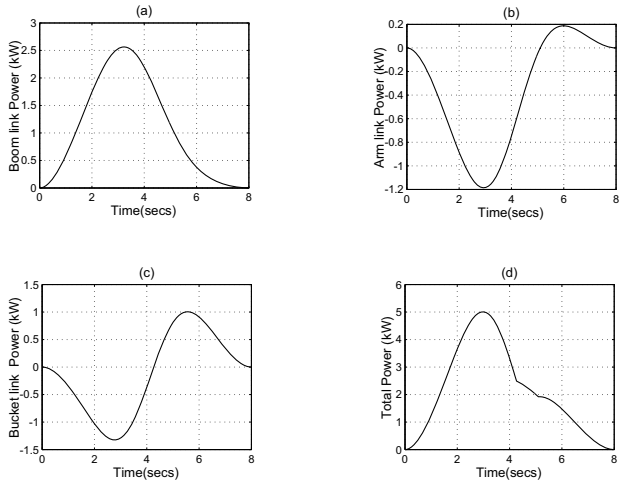

Fig. 10. **(a)** Boom joint power **(b)** Arm joint power **(c)** Bucket joint power **(d)** Total joints power ;when the bucket is digging a sandy-loom soil and at the initial cycle times

The peak value for the total power consumption when the bucket is digging a sandy-loom soil is shown to be approximately $5kW$ $(6.7hp)$. This value is greater than the power rating of the engine $(6.5hp)$ which is to drive the hydraulic pump, implying that, the digging operation cannot be achieved under the given link trajectories without exceeding the power capacity of the prime mover.

The power consumption as seen in (21)-(24) depends on the joint torque requirements and the angular velocities of the links. Two options are available to reduce the total power requirement of the manipulator. These are;

- Reduce the joint torque requirements for the manipulator, by reducing the mass properties of the links and/or reducing the force exerted to the ground by the bucket.
- Increase the cycle times of the link trajectories. This means that the pump flow rate capacity will be reduced.

In this work, the second option of increasing the cycle times of the link trajectories was used. Generally, the cycle time has a direct impact on the flow rate requirements relative to the link/actuator motion requirements, and on the power requirement of the manipulator. As seen in (19) increasing the cycle time t_f will decrease the link velocities, and this will subsequently reduce the power requirement and also the flow rates requirement.

The optimum cycle time necessary to ensure that the power requirement for the manipulator motion when the bucket is digging a sandy-loom soil is reduced was found to be $10s$. Fig. 11 shows the new power requirement profiles for the manipulator.

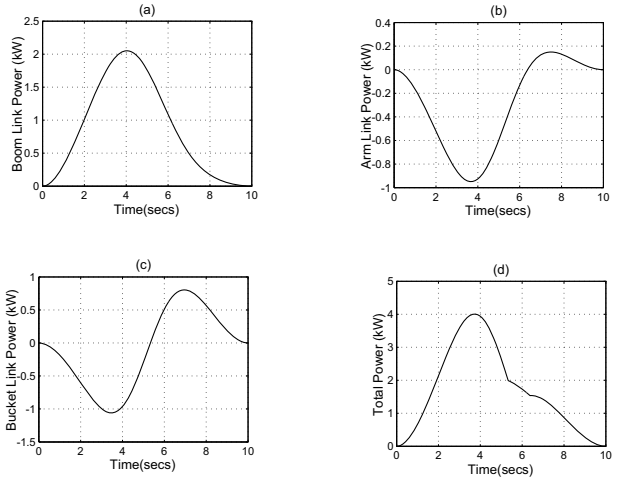

Fig. 11. **(a)** Boom joint power **(b)** Arm joint power **(c)** Bucket joint power **(d)** Total joints power ;when the manipulator is digging a sandy-loom soil and at the optimal cycle times

D. Sizing the Hydraulic Actuators and Valves based on Inverse Dynamics

An important application of the inverse dynamic modeling of hydro-mechanical systems is the sizing of hydraulic components. In this section, the optimal sizes of the actuator pistons as well as the optimal sizes of the spool valve orifice ports of the boom, arm, and bucket cylinders are determined. For this purpose, the pressure drop profiles across the cylinders and valves need to be plotted from the inverse dynamics.

1) Pressure Drop Profiles: The hydraulic forces required to produce the torques necessary for manipulator motion results in corresponding pressure drops across the hydraulic cylinders. The expressions for the pressure drop in the boom cylinder,

Δp_{bo}, arm cylinder, Δp_a, and bucket cylinder, Δp_{bu} are approximated using equations below;

$$\Delta p_{bo} = \frac{F_{cy_{bo}}}{A_{p_{bo}}} \quad (25)$$

$$\Delta p_a = \frac{F_{cy_a}}{A_{p_a}} \quad (26)$$

$$\Delta p_{bu} = \frac{F_{cy_{bu}}}{A_{p_{bu}}} \quad (27)$$

The cylinder forces are related to the joint torques by the manipulator jacobians which for the manipulator in consideration are derived in [19]. The pressure drop profiles across the cylinders when the bucket is digging a sandy-loom soil are shown in Fig. 12.

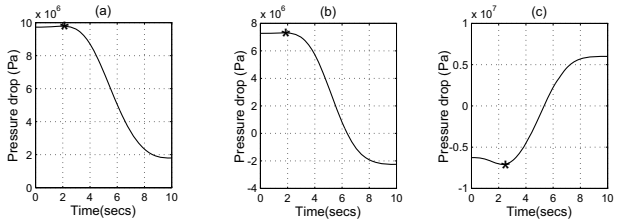

Fig. 12. The Pressure drop profiles across the cylinders, when the bucket is digging a sandy-loom soil and at original piston diameters; **(a)** Boom cylinder **(b)** Arm cylinder **(c)** Bucket cylinder

Neglecting line pressure drops, the pressure drops at the corresponding valves are approximated as;

$$\Delta p_{bo_v} = p_s - |\Delta p_{bo}| \quad (28)$$

$$\Delta p_{a_v} = p_s - |\Delta p_a| \quad (29)$$

$$\Delta p_{bu_v} = p_s - |\Delta p_{bu}| \quad (30)$$

Where p_s is the operating pressure. The pressure drop profiles at the valves for the case when the bucket is digging a sandy-loom soil is shown in Fig. 13.

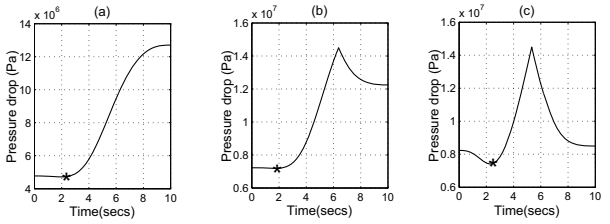

Fig. 13. The Pressure drop profiles across the cylinder valves, when the bucket is digging a sandy-loom soil and at original piston diameters; **(a)** Boom cylinder valve **(b)** Arm cylinder valve **(c)** Bucket cylinder valve

2) Actuator Sizing: As shown in (25)- (27) the cross sectional area of the piston of a cylinder determines the pressure drop across the cylinder during the working stroke, which is considered to be the extension stroke. And from (28)-(30) the maximum possible pressure drop (Δp_{max}) across a given cylinder should be equal to the supply pressure (p_s), that is,

$$\Delta p_{max} = p_s \quad (31)$$

- If $\Delta p_{max} < p_s$, then this implies that the supply pressure is not used maximally and hence there is no need of such a high pump pressure since the cylinder is oversized.
- If $\Delta p_{max} > p_s$, then the pressure drop across the valve becomes negative and this will result to a negative flow rate through the valve. This is not possible practically and implies that the cylinder is undersized.

As seen in Fig. 12, the maximum pressure drops across the cylinders (points with asterisks) are less than the supply pressure of $p_s = 14.5MPa$. This is also shown in Fig. 13 where at the point of maximum pressure drop for all the cylinders (points with asterisks), the pressure drops across the corresponding valves do not equal to zero. Therefore it can be concluded that the boom, arm and bucket cylinders are oversized.

The optimal cylinder piston sizes were determined by tuning the piston sizes until that instant when the maximum pressure drops equaled the supply pressure for all the cylinders. These values were found to be precisely 52.2mm, 45.1mm and 40.9mm for the boom, arm and bucket cylinders respectively, as shown in Fig. 14. The optimal piston diameters values of the cylinders were rounded to the next imperial values which are available in the market as 57.15mm ($2\frac{1}{4}$in), 50.8mm (2in) and 44.45mm ($1\frac{3}{4}$in) for the boom, arm and bucket cylinders respectively.

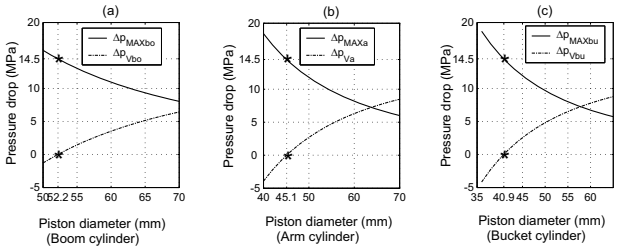

Fig. 14. The pressure drops versus piston diameters; **(a)** Boom cylinder **(b)**Arm cylinder **(c)** Bucket cylinder

3) Valve Sizing: A valve is properly sized when it can supply the demanded flow at the required pressure drop across it. Therefore to size a valve, flow and pressure requirements must be obtained as a function of time for a given task. Obviously, the task becomes more demanding when the manipulator's bucket is digging a trench.

The flow through the valves for the three actuators is obtained from the following equations,

$$Q_{bo} = A_{p_{bo}} \dot{x}_{p_{bo}} \quad (32)$$

$$Q_a = A_{p_a} \dot{x}_{p_a} \quad (33)$$

$$Q_{bu} = A_{p_{bu}} \dot{x}_{p_{bu}} \quad (34)$$

where Q is the flow to the cylinder, A_p is the average area of the cylinder piston, and $\dot{x}_p$ is the velocity of the cylinder piston.

The pressure drops across the valves is obtained from (28)-(30). These equations can be used to plot valve flow versus valve pressure drop for the desired end-point trajectories.

The resulting $Q - \Delta p$ curve should lie below the valve pressure-flow characteristics at full valve opening, $Q_v - \Delta p_v$, typically a curve described by a relationship of the form;

$$Q_v = C_d A_O \sqrt{\frac{2}{\rho} \Delta p_v} \tag{35}$$

Where Q_v is the flow rate through a valve, Δp_v is the pressure drop across the valve, C_d is the discharge coefficient, ρ is the fluid density and A_O is the area of the orifice opening.

If $Q - \Delta p$ curve does not lie below the valve pressure-flow characteristic curve at full valve opening, then the pressure drop across the valve is less since the pressure drop across the actuator is large. Therefore, the valve flow rate is not able to provide the motion to the manipulator at the specified speed at a particular operating pressure. In this case a valve of larger capacity must be specified, or the value of the operating pressure increased. Fig. 15, shows the typical plots of such curves when the bucket is digging a sandy-loom soil.

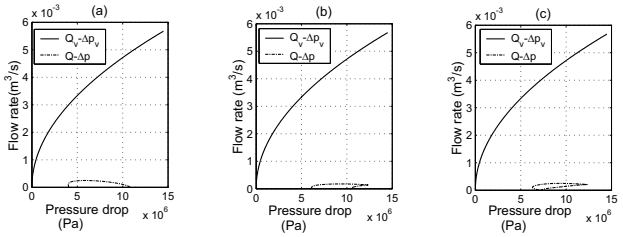

Fig. 15. Pressure drops versus flow curves, when the bucket is digging a sandy-loom soil and at the initial sizes of the valve's orifices; **(a)** Boom cylinder valve **(b)** Arm cylinder valve **(c)** Bucket cylinder valve

As seen in Fig. 15, the $Q - \Delta p$ curves for all the cylinder valves are far below the valve characteristic curves, hence it can be concluded that the manipulator will be able to operate with the selected valves, although the valve orifice ports are seen to be oversized. An optimal orifice port size should ensure that the peak value of the $Q - \Delta p$ curve is well near the valve characteristic curve.

The optimal orifice port sizes were determined by tuning the radii of the ports until that instant when the peak values of the $Q - \Delta p$ curves for all the valves are well below the characteristic curves. These values were found to be precisely equal to 1.5mm for all the cylinder valves. The optimal port diameter values of 3mm were rounded to the next imperial values which are available in the market as 3.175mm ($\frac{1}{8}$in). The resulting pressure drop versus flow curves are shown in Fig. 16.

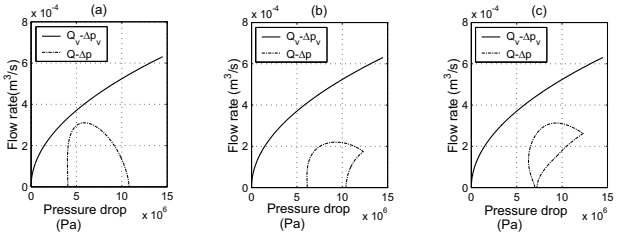

Fig. 16. Pressure drops versus flow curves, when the bucket is digging a sandy-loom soil and at the optimal sizes of the valve's orifices; (a) Boom cylinder valve (b)Arm cylinder valve (c) Bucket cylinder valve

IV. Conclusion

Bond graph modeling tool has been applied to model the mechanical dynamics of an excavating manipulator which was modeled as a 3 degree of freedom planar manipulator. This was done by applying forward recursive equations similar to those applied in iterative Newton-Euler method only to determine the centroid velocities of the links, unlike in Newton-Euler method which requires extra recursive computations to determine the centroid accelerations of the links. A dynamic model resulted after representing the horizontal and vertical velocities of the links in bond-graphic form, while considering the momenta and weights of the links as the bond graph elements. On the other hand, Newton-Euler method requires backward recursion to be performed in order to obtain a dynamic model. This showed that the bond graph method reduces significantly the number of recursive computations required to be performed to a manipulator for a dynamic model to result, and therefore it can be concluded that bond graph method is more computationally efficient than the Newton-Euler method in developing dynamic models of manipulators. Based on the developed model, valve-sizing and actuator-sizing methodologies were briefly outlined and used to obtain the optimal sizes of the ports of the spool valves as well as the optimal sizes of the pistons of the hydraulic cylinders.

References

[1] J. Denavit, and R. S. Hartenberg, "A kinematic notation for lower-pair mechanisms based on matrices," *Journal of Applied Mechanics*, pp. 215–221., 1955.

[2] K.S. Fu, R. C. Gonzalez, and C. S. Lee, *Robotics: Control, Sensing, Vision and Intelligence*. McGraw Hill Book Publishing Company, 1987.

[3] J. J. Craig, *Introduction to Robotics: Mechanics and Control*. Addison-Wesley Publishers, USA, 1986.

[4] V. Anand, H. Kansal, and A. Singla, "Some aspects in bond graph modeling of robotic manipulators: Angular velocities from symbolic manipulation of rotation matrices," Technical Report, Department of Mechanical Engineering, Sant Longowal Institute of Engineering and Technology, 2003.

[5] H. M. Paynter, *Analysis and Design of Engineering Systems*. MIT Press Publishers, Cambridge, 1961.

[6] D. C. Karnopp, D. L Margolis, and R. C. Rosenberg, *System Dynamics: Modelling and Simulation of Mechatronic Systems*. John Wiley and Sons Publishers, Newyork, 2000.

[7] D. C. Karnopp, D. L. Margolis, and R. C. Rosenberg, *System Dynamics; A Unified Approach*. John Wiley and Sons Publishers, Newyork, 2nd ed., 1990.

[8] D .C. Karnopp and R. C. Rosenberg, *Introduction to Physical System Dynamics*. McGraw Hill Publishers, Newyork, 1983.

[9] P. Breedveld, "Bond graphs," in *Encyclopedia of Life Support Systems, Modeling and Simulation*, 2003.

[10] P. Gawthrop and L. Smith, *Metamodeling: Bond Graphs and Dynamic Systems*. Prentice Hall International Publishers, UK Limited, 1996.
[11] F. Fakri, A. Rocaries, and A. Carrierre, "A simple method for conversion of bond graph models in representation by block diagrams," in *1997 Proc. International Conference on Bond Graph Modeling and Simulation*.
[12] J. F. Broenink, "Introduction to Physical Systems Modeling with Bond Graphs," Technical Report, Department of Electrical Engineering, University of Twente, Netherlands, 1996.
[13] O. M. Muvengei, "Design of an excavating mechanism to be used with juja diesel tractor jk01," Design Innovation, Department of Mechanical Engineering, J.K.U.A.T, 2006.
[14] A. Koivo, "Kinematics of excavator (back hoe) for transfering surface materials," *Journal of Aerospace Engineering*, vol. 7(1), pp. 7–31, 1994.
[15] J. Y. Luh, M. W. Walker, and R. P. Paul, "On-line computational scheme for mechanical manipulators," *Journal of Dynamic Systems, Measurement and Control*, vol. 120, pp. 69–76, 1980.
[16] H. N. Cannon, "Extended earthmoving with an autonomous excavator," MSc. thesis, Robotics Institute, Carnegie Mellon University, Pittsburgh, 1999.
[17] H. Q. Nguyen, *"Robust low level control of robotic excavation"*. PhD. thesis, Australian Centre for Field Robotics, The University of Sydney, 2000.
[18] S. Sarkar, "Dynamic modeling of an articulated forestry machine for simulation and control," MSc. thesis, Department of Mechanical Engineering, McGill University, Canada, 1996.
[19] O. M. Muvengei, "Simulation of the dynamic behavior of an excavator due to interacting mechanical and hydraulic dynamics," MSc. thesis, Department of Mechanical Engineering, JKUAT, Kenya, 2008.